Future water storage changes over the Mediterranean, Middle East, and North Africa in response to global warming and stratospheric aerosol intervention

Abolfazl Rezaei[1,2], Khalil Karami[3], Simone Tilmes[4], John C. Moore[5]

[1] Department of Earth Sciences, Institute for Advanced Studies in Basic Sciences (IASBS), Zanjan 45137-66731, Iran. arezaei@iasbs.ac.ir; abolfazlrezaei64@gmail.com.

[2] Center for Research in Climate Change and Global Warming (CRCC), Institute for Advanced Studies in Basic Sciences (IASBS), Zanjan 45137-66731, Iran

[3] Institut für Meteorologie, Stephanstraße 3, 04103 Leipzig, Germany. khalil.karami@uni-leipzig.de

[4] National Center for Atmospheric Research, Boulder, CO, USA. tilmes@ucar.edu

[5] Arctic Centre, University of Lapland, Rovaniemi, 96101, Finland. john.moore.bnu@gmail.com

Abstract

Water storage plays a profound role in the lives of people across the Middle East and North Africa (MENA) as it is the most water stressed region worldwide. The lands around the Caspian and Mediterranean Seas are simulated to be very sensitive to future climate warming. Available water capacity depends on hydroclimate variables such as temperature and precipitation that will depend on socioeconomic pathways and changes in climate. This work explores changes in both the mean and extreme terrestrial water storage (TWS) under an unmitigated greenhouse gas (GHG) scenario (SSP5-8.5) and stratospheric aerosol intervention (SAI) designed to offset GHG-induced warming above 1.5 °C and compares both with historical period simulations. Both mean and extreme TWS are projected to significantly decrease under SSP5-8.5 over the domain, except for the Arabian Peninsula, particularly in the wetter lands around the Caspian and Mediterranean Seas. Relative to global warming, SAI partially ameliorates the decreased mean TWS in the wet regions while it has no significant effect on the increased TWS in drier lands. In the entire domain studied, the mean TWS is larger under SAI than pure greenhouse gas forcing, mainly due to the significant cooling, and in turn, a substantial decrease of evapotranspiration under SAI relative to SSP5-8.5. Changes in extreme water storage excursions under global warming are reduced by SAI. Extreme TWS under both future climate scenarios are larger than throughout the historical period across Iran, Iraq, and the Arabian Peninsula, but the response of the more continental eastern North Africa (NA) hyper-arid climate is different from the neighboring dry lands. In the latter case, we note a reduction in the mean TWS trend under both GHG and SAI scenarios, with extreme TWS values also showing a decline compared to historical conditions.

Keywords: Mean and extreme water storage; SSP5-8.5; Stratospheric Aerosol Intervention; Global warming; MENA region, Caspian and Mediterranean Seas

500-character non-technical text

Water storage (WS) plays a profound role in the lives of people in the Middle East and North Africa and Mediterranean climate "hot spots". Simulated is WS changed by greenhouse gas (GHG) warming with and without stratospheric aerosol intervention (SAI). WS significantly increases in the Arabian Peninsula and decreases around Mediterranean under GHG. While SAI partially ameliorates the GHG impacts, projected WS increases in dry regions and decreases in wet areas relative to the present climate.

1. Introduction

The Middle East and North Africa (MENA), with 6% of the world's population, are currently among the most water-stressed regions worldwide (Fragaszy et al., 2020). The dry climate, intensifying droughts, increasing population, and water over-extraction particularly across the Middle East (World Bank, 2017), make it home to 12 of the 17 most water-stressed countries on the planet (Hofste et al., 2019). Water availability is crucial for sanitation (Reiter et al., 2004), economic activity (UNESCO, 2003), ecosystems (Shiklomanov and Rodda, 2003), and hydrological systems (Mooney et al., 2005).

The MENA region has the largest expected economic losses from climate-related water scarcity, robustly estimated at 6–14 % of Gross Domestic Product (GDP) by 2050 (World Bank, 2017). MENA's terrestrial water storage (TWS) is being intensively extracted and may act as a flashpoint for conflict (Famiglietti, 2014). TWS incorporates all water on the land surface (snow, ice, water stored in the vegetation, river, and lake water) and in the subsurface (soil moisture and groundwater). Beyond anthropogenic activities, natural climate variability such as drought frequency affects water storage and agriculture, which then impacts food security (Fragaszy et al., 2020). The Middle East is especially prone to severe and sustained droughts due to its location in the descending limb of the Hadley circulation and associated dry and semiarid climate (Barlow et al., 2016). The 1998-2012 14-year period was the worst drought in the past 900 years (Cook et al., 2016). Because the saturated vapor pressure of air is largely controlled by temperature, any change in temperature, as well as precipitation, substantially affects (Konapala et al., 2020; Ajjur and Al-Ghamdi, 2021; Hobeichi et al., 2022) the water storage capacity available to supply the increasing water demand in the region (Lian,

2021). The MENA region, having both low precipitation and high evaporation, is very vulnerable to climate change (Giorgi, 2006; Lelieveld et al., 2012; Tabari and Willems, 2018; Zittis et al., 2019). MENA water storage is therefore particularly sensitive to any perturbation of the water cycle imposed by global warming.

GHG warming has already adversely affected water resources in the MENA region (Wang et al., 2018) and is simulated to intensify water competition between states (Arnell, 1999) in the future. Although global warming is expected to increase precipitation and soil moisture across MENA (Cook et al., 2020), it will decrease runoff and groundwater recharge by larger amounts (Milly et al., 2005; Shaban, 2008; Suppan et al., 2008). Using the GHG emission scenario A1B simulated by nine CMIP3-class climate models, Droogers et al. (2012) projected that 22% of the future annual water shortage, 199 km^3 in 2050 in MENA, will be due to global warming. 17 global climate models from Coupled Model Intercomparison Project Phase 6 (CMIP6) under SSP5-8.5 simulate a significant increase in precipitation ($+0.05$ to 0.3 ∓ 0.1 mm day^{-1}) over South-Eastern Saharan Desert in NA by the end of the century (Arjdal et al., 2023). They also projected that the total soil moisture would increase over Southern Saharan Desert under the SSP5-8.5 (6 to 20%) and SSP2-4.5 (4 to 14%). Based on TWS data from eight global climate models participating in CMIP6, a broad part of the dry MENA region tends to be wetter under SSP5-8.5 over 2071-2100 (Xiong et al., 2022). GHG-driven groundwater storage depletion in the Middle East during the 21st century will far exceed that during the 20th century due to the increased evapotranspiration (ET) and reduced volume of snowmelt (Wu et al., 2020).

Although MENA's adjacent densely populated region, the Mediterranean, has a better water storage state, it is projected to substantially suffer from reduced water availability under future GHG climate scenarios (Lionello et al., 2006). This is due to both projected significant decreases in rainfall (Azzopardi et al., 2020) and large increases in demand for irrigation water by the end of the 21st century (Fader et al., 2016). The precipitation and water availability in the Mediterranean region, to the northwest of the MENA, is also projected to be highly sensitive to global warming, particularly regarding water availability (Lionello et al., 2006), having the largest differences in the water availability between 1.5 and 2°C warming scenarios globally (Schleussner et al., 2016). Global warming decreases Mediterranean groundwater recharge according to simulations under the IPCC A2 and B2 scenarios simulated using ECHAM4 and HadCM3 models (Döll and Flörke, 2005). Runoff is decreased by 10-30% according to 12 models such as CCSM3, and ECHAM5/MPI-OM (Milly et al., 2005), and soil moisture z-scores (obtained by taking the difference from the average and then

dividing it by the standard deviation of the time series from the baseline period) by -1 to -4 in warm seasons according to simulations under SSP1-2.6, SSP2-4.5, SSP3-7.0, and SSP5-8.5 (Cook et al., 2020). Water availability in turn is lowered by 8-28% for a warming of 2 °C as simulated by 11 CMIP5-class models by Schleussner et al. (2016). Likewise, Döll et al. (2018) found a strong drying in the Mediterranean region under global warming since the largest precipitation decreases worldwide were simulated in this region under SSP1-2.6, SSP2-4.5, SSP3-7.0, and SSP5-8.5 scenarios (Cook et al., 2020). CMIP5 model rsults also confirm that the global warming (RCP2.6 and RCP6.0) substantially decreases the TWS in the Mediterranean by the mid- (2030-2059) and late- (2070-2099) twenty-first century (Pokhrel et al., 2021).

If global mean surface temperature rises to exceed 1.5 °C above the preindustrial mean temperature, severe global consequences, and societal problems can be expected (Masson-Delmotte, 2022). Solar radiation modification (SRM), a form of intervention to cool the climate by reflecting sunlight, has been proposed as a potential method of limiting global temperature rises and the associated impacts of increased GHG emissions. SRM may be the only way to keep or reduce surface temperatures to 1.5 °C given the reality of the GHG mitigation measures that have been agreed upon to date (MacMartin et al., 2022). Simulations have shown a 2% decrease in total solar irradiance roughly offsets global warming due to a doubling of CO_2 concentrations, and continuous injections of 10-18 Tg SO_2 per year would lead to a cooling of about 1 °C after several years (WMO, 2022). This is consistent with observed surface cooling after large volcanic eruptions, such as the 1991 Mt Pinatubo eruption which produced cooling of about 0.3 °C over a 2-3 year period (e.g., IPCC, 2021).

Many global climate models have simulated SRM in the form of stratospheric aerosol intervention (SAI). Model studies include the Stratospheric Aerosol Geoengineering Large Ensemble Project GLENS (e.g., Cheng et al., 2019; Simpson et al., 2019; Abiodun et al., 2021), the Geoengineering Model Intercomparison Project (Kravitz et al., 2013; Tilmes et al., 2013), as well as others (e.g., Bala et al., 2008; Jones et al., 2018; Muthyala et al., 2018). Compared with global warming, SAI decreases mean global precipitation (Govindasamy and Caldeira, 2000; Bala et al., 2008; Robock et al., 2008; Cheng et al., 2019; Simpson et al., 2019) as well as both the intensity and frequency of precipitation extremes caused by GHG-induced climate change (Tilmes et al., 2013; Muthyala et al., 2018). Dagon and Schrag (2016) is a rare article that focuses on the spatial variability of runoff and soil moisture responses to SRM. Although solar geoengineering weakens the global hydrologic cycle (e.g., Bala et al., 2008; Tilmes et al., 2013; Ricke et al., 2023), its regional impacts are method- and strategy-dependent

(Ricke et al., 2023) with potentially substantial changes in the regional precipitation patterns (Ricke et al., 2010; Tilmes et al., 2013; Crook et al., 2015; Dagon and Schrag, 2016, Tilmes et al., 2020). While differences in temperature fields vary relatively smoothly with radiative forcing, precipitation patterns are far more variable being dependent on atmosphere/ocean/land surface coupling on a wide range of spatial and temporal scales. Furthermore, SAI simulations rely on many model-specific details and parameterizations that tend to produce larger across-model differences than simulations using simpler forms of SRM (Visioni et al., 2021). While SAI may counteract the annual-mean water availability changes over land forced by GHG, it is not easy to offset the regional consequences, especially in the hydrological cycle, such as the Amazonian drying trend and its reduced precipitation, evaporation, and precipitation minus evaporation (Jones et al., 2018).

Although the MENA region and the adjacent Mediterranean region are known to be a "hot spot" for climatic change (Giorgi and Lionello, 2008; Bucchignani et al 2018), little has been done on potential changes in TWS across MENA especially under SRM climates. This study fills that knowledge gap and explores the changes that may occur in TWS under i) a high GHG emissions scenario, ii) the same GHG scenario combined with SAI designed to globally neutralize the GHG radiative forcing, and iii) compares both future climates with the historical conditions (1985-2014) across the Mediterranean, Middle East, and northern Africa.

2. Data and Methods

2.1. Study Area

The study area is composed of MENA and southern Europe to its north including the Caspian and Mediterranean Seas. MENA covers the large region from Morocco in the west to Iran in the east, containing all the Maghreb and the Middle Eastern countries from the 15^0N to 45^0N latitude and from 20^0W to 63^0E longitude (Fig. 1). As well as a water-stressed region, MENA, is a worldwide hot spot for exacerbated extreme temperatures, aridity conditions, and drought (Giorgi and Lionello, 2008; Bucchignani et al., 2018). According to the Koppen Climate Classification System (Peel et al., 2007), MENA broadly has a hot and arid climate except for the coastal regions and highlands. Most of northern Africa (NA) has a desert climate and 90% is covered by the Saharan Desert. The 2 m air temperature rises to 50°C in summertime while the annual mean precipitation is less than 25 mm (Faour et al., 2016). The Arid Steppe climate predominates in Morocco, Algeria and Tunisia with cold winters (Faour et al., 2016) except for the Atlas Mountains which are cooler and wetter (annual mean precipitation of ~500mm).

Across the Middle East, the largest amount of precipitation falls in four main regions: the coastal eastern Mediterranean Sea, the south coast of the Caspian Sea, the western sides of the Zagros Mountains across Iran and Iraq, and the southern tip of the Arabian Peninsula. The Middle East also contains several major deserts having little to no precipitation: the Lut and Kavir deserts in the south-east and north-central regions in Iran, the Arabian Desert, the Syrian Desert, and the Negev in south-eastern corner of the Mediterranean Sea. Middle East precipitation often originates from moisture coming from the west over the Mediterranean Sea (Evans and Smith, 2006). The Red Sea and the Persian Gulf are also source regions for the heaviest precipitations across the area.

The Mediterranean area has mild wet winters and warm to hot, dry summers as well as a complicated morphology, owing to the many steep orogenic structures, distinct basins and gulfs, along with islands and peninsulas of various sizes (Lionello et al., 2006).

Based on its full range of climate types, we divided the study area into six sub-regions (R1 to R6) to explore the changes in hydroclimate variables under both global warming and SAI scenarios (Fig. 1). The regions R1 to R6 respectively refer to the lands around the Caspian Sea, eastern Middle East (largely containing Iran and Iraq), Mediterranean area, Arabian Peninsula, eastern NA, and western NA. The simulated present-day climatology (1985-2014) of each region for different hydrological quantities is summarized in Table 1.. Potential evapotranspiration (ET) is the amount of evaporation that would occur if a sufficient water source were available. The Thornthwaite method was used to calculate the potential ET based on the monthly mean temperature and latitude data for each grid. Evaporation from both soil and canopy and transpiration are summed up to obtain the real ET, which is the quantity of water actually removed from a surface by evaporation and transpiration. The lands around the Caspian and Mediterranean Seas with a cooler climate, have the highest precipitation and real ET while more continental eastern NA with hyper-arid climate (with annual precipitation less than 100 mm) has the lowest precipitation, real ET, soil moisture, and TWS. The lands around the Caspian Sea have the highest soil moisture and TWS. More continental refers to an area with characteristics that are typical of continental climates and is less influenced by the moderating effects of nearby oceans.

Table 1. The medians of precipitation, temperature, real evapotranspiration (ET), soil moisture, terrestrial water storage (TWS), and potential ET over each region (R1 to R6, see Fig. 1) during the historical period according to the model outputs. The results for global warming and SAI are further shown in Table S1.

Region	R1	R2	R3	R4	R5	R6
Precipitation (mm/yr)	321	182	479	78	48	112
Temperature (^{0}C)	14.2	20.5	17.2	27.0	23.7	25.3
Real ET (mm/yr)	419	187	388	72	50	112
Soil moisture (Kg/m^2)	1846	1771	1572	1353	1155	1287
TWS (Kg/m^2)	2091	1776	1623	1348	1167	1313
Potential ET (mm/yr)	74	123	74	210	143	185

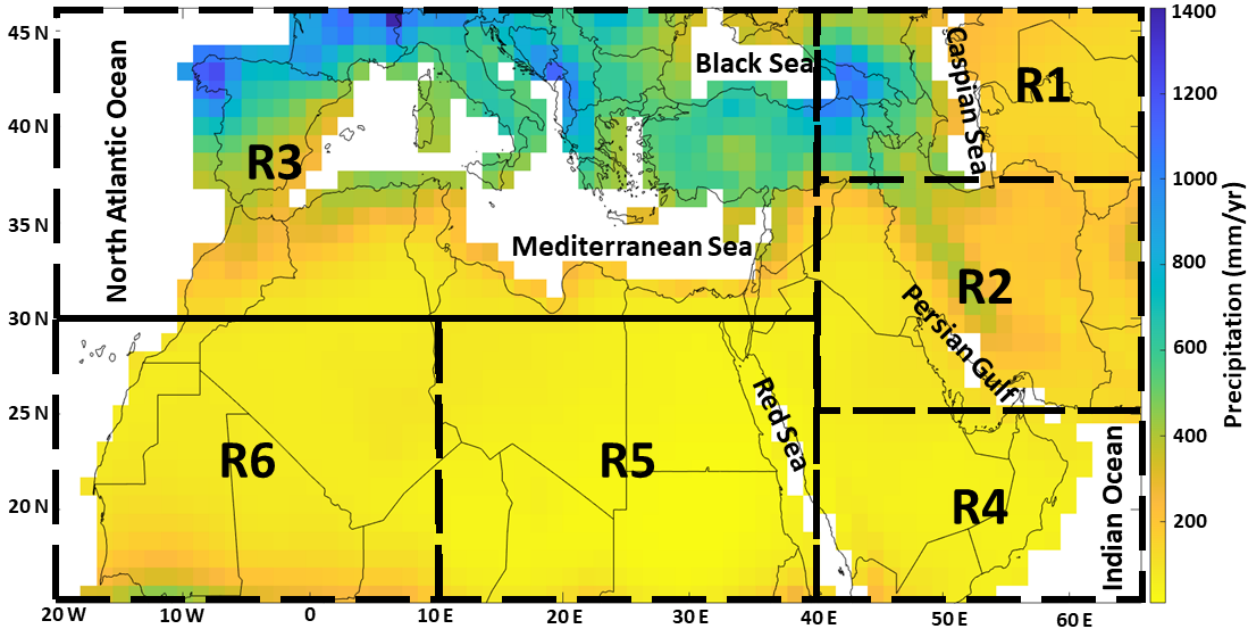

Figure 1. The MENA's annual precipitation map during the historical period. Regions R1 to R6 largely refer to the lands around the Caspian Sea, the eastern Middle East (largely containing Iran and Iraq), the Mediterranean area, Arabian Peninsula, eastern North Africa (NA), and western NA, respectively.

2.2. Model simulations and scenarios

We examined the data from the NCAR Community Earth System Model version 2- Whole Atmosphere Community Climate Model Version 6 (CESM2(WACCM6)) that simulated the CMIP6 (Eyring et al., 2016) scenarios. CESM2 ranks among the top nine models known for their accuracy in simulating

global precipitation patterns, based on the Hellinger distance metric, which compares the bivariate empirical densities of CESM2 with those of 34 CMIP6 models, against historical precipitation data sourced from the Global Precipitation Climatology Centre (GPCC) (Abdelmoaty et al., 2021). CESM2 has precipitation biases about 20% lower than CESM1 (Danabasoglu et al., 2020). CESM2(WACCM6) has an interactive stratospheric aerosol treatment (Danabasoglu et al., 2020) that is consistent with observations (Mills et al., 2016). For global terrestrial ET, the CESM2(WACCM6) ranked as the second-best model among 19 CMIP6 models (Wang et al., 2021). Furthermore, CESM2(WACCM6), reproduced the observed global land carbon trends remarkably well (Danabasoglu et al., 2020), and includes a full ocean model (Parallel Ocean Program version 2, POP2) to simulate the response of stratospheric aerosol change in the climate.

CESM2 also demonstrates satisfactory performance in simulating historical climate conditions within the study area. In the evaluation by Babaousmail et al. (2021), which assessed 15 CMIP6 models in replicating monthly rainfall patterns spanning from 1951 to 2014 in NA, CESM2(WACCM6) emerged as one of the top-performing models. It accurately captured rainfall peaks across the region, albeit with a slight overestimation (ranging from 5 to 10 mm/month) in the southern areas and a slight underestimation (ranging from 0 to 20 mm/month) in the northern regions. Despite these minor deviations, CESM2(WACCM6) was recognized as one of the models for well simulating precipitation patterns across NA, achieving a Taylor skill score of 0.62. Evaluation of CESM2(WACCM6) across the Mediterranean coasts placed it at the 9th and 17th positions out of 31 CMIP6 models for its performance in simulating temperature and precipitation (Bağçaci et al., 2021). Furthermore, when it comes to simulating precipitation relative to observational data for northeastern Iran during the period of 1987-2005, CESM2 stood out as the top-performing model among six CMIP6 models (Zamani et al., 2020). Assessing the representation of spatial and temporal variations in historical precipitation from 1980 to 2014 across Africa and the Arabian Peninsula, the CMIP6 multi-mean ensemble (inclusive of CESM2(WACCM6)) demonstrated reasonable performance, as highlighted in Nooni et al. (2023).

The SAI simulation we use (SSP5-8.5-SAI) is designed to employ SAI together with the high GHG emissions scenario, SSP5-8.5 with the target of limiting the mean global temperatures to 1.5°C above the pre-industrial (1850–1900) conditions (Tilmes et al., 2020). Under SSP5-8.5 forcing, Tilmes et al. (2020) projected this threshold is exceeded around the year 2020 in CESM2(WACCM6). The atmospheric component of CESM2(WACCM6) has a resolution of 1.25° in longitude and 0.9° in

latitude. The experiment injects SO_2 at 180° longitude at four predefined latitudes (30°N, 30°S, 15°N, and 15°S) at around 25 km in 15°N/S and around 22 km at 30°N/S as suggested by Tilmes et al. (2018), using a feedback control algorithm to maintain not just the global mean temperature, but the interhemispheric and equator-to-pole temperature gradients (Tilmes et al., 2020). For SSP5-8.5-SAI, most of the sulfur mass was injected at 15°S, some at 15°N and 30°S, and very little at 30°N. We used the monthly TWS (the sum of snow water equivalent and soil moisture (Wu et al., 2021)), precipitation, temperature, water evaporation from soil and canopy, transpiration, soil moisture, and leaf area index (LAI) data from all five ensemble members (r1 to r5) of the SSP5-8.5 scenario and the three available ensemble members (1-3) of SSP5-8.5-SAI. The results for variables other than TWS are shown in the Supplementary Information. For the historical period, we used all three available realizations (r1 to r3) from CESM2(WACCM6). For the anomaly analysis relative to historical conditions and the multiple linear regression models, we used the first three ensembles of SSP5-8.5, consistent with the three available historical members. We compare the GHG and SAI scenarios over 2071-2100 with the 1985-2014 historical period.

We focused on the historical period from 1985 to 2014 rather than the entire historical dataset spanning from 1850 to 2100 for several reasons. Firstly, recent historical climate data may exhibit less uncertainty, given that additional meteorological stations with improved data quality are available to be used for model calibrations (Zhang et al., 2020). Secondly, this selected historical period offers valuable insights into the observable impacts of climate change, which are highly pertinent to present-day societal and environmental challenges. These insights are of utmost importance to policymakers and communities alike. Thirdly, the chosen historical 30-year time period aligns with the 30-year periods considered for the GHG emissions and SAI scenarios, ensuring consistency in our statistical analysis. We focus on the 2071-2100 future period because the anticipated changes in TWS driven by GHG emissions are expected to be more pronounced during this time frame (Pokhrel et al., 2021). Furthermore, the SAI forcing is strongest in the later period of the simulation and is expected to produce a more significant result.

2.3. Return periods

We are interested in climate extremes, not only changes in means. Therefore, we examine how the frequency of events of some particular levels are likely to change under different scenarios. We use the generalized extreme value (GEV) distribution function to estimate the probability distribution function of the TWS extremes. A return period is an estimated average time between events such as

floods or river discharge flows. It is calculated by generating the 95% normal-approximate confidence intervals in accordance with the mean and variance of the variable (here TWS).

The GEV probability density and cumulative distribution functions are defined as (Gilleland, 2020):

$$g(z)=\frac{1}{\sigma}t(z)^{1+\xi}e^{-t(z)};\ G(z)=e^{-t(z)};\ t(z)=\begin{cases}\left\{1+\xi\left(\frac{z-\mu}{\sigma}\right)\right\}^{-1/\xi}, & \xi\neq 0\\ e^{-\left(\frac{z-\mu}{\sigma}\right)}, & \xi=0\end{cases} \quad (1)$$

For $\xi\neq 0$, we have $t(z)^{1+\xi}=\left\{1+\xi\left(\frac{z-\mu}{\sigma}\right)\right\}^{-(1+1/\xi)}$ and for $\xi=0$, the x domain restricted to $\xi\left(\frac{z-\mu}{\sigma}\right)>-1$. The GEV distribution is parameterized using ξ, μ, and σ which are the shape, location, and scale parameters, respectively and analogous to the skewness, mean and standard deviation. We assume that the GEV is the valid distribution function for variables $z_1, \ldots, z_n$ representing the annual maximum return TWS levels, where the quantiles of the distribution function give the return levels, z_p. The return levels are the solutions to $G(z_p)=1-p$, which yields (Gilleland, 2020):

$$z_p=\begin{cases}\mu-\frac{\sigma}{\xi}[1-\{-\ln(1-p)\}^{-\xi} & for\quad \xi\neq 0\\ \mu-\sigma\ln\{-\ln(1-p)\} & for\quad \xi=0\end{cases} \quad (2)$$

p is probability corresponding to z_p. The return period is obtained as:

$$return\ \ period\ (i)=1/(1-cdf\ (i)) \quad (3)$$

where *cdf* is the cumulative distribution function. We also calculated the 95% asymptotic lower and upper confidence intervals based on the Kolmogorov-Smirnov statistic (Doksum and Sievers, 1976). We used the concatenated TWS anomaly data for the historical period, high GHG emissions, and SAI scenarios to analyze the return periods. As an example, the relationship between empirical quantiles and model quantiles as well as the probability density versus quantiles for the regions R2 and R5 are shown in Figs. S1 and S2.

2.4. Multiple linear regression (MLR) model

We want to analyze how the primary driving climate fields (surface air temperature, precipitation, ET, and LAI (i.e., vegetation coverage)) for TWS vary spatially and among the different scenarios

(Zhang et al., 2022). We use a simple multiple linear regression (MLR) model with TWS as the dependent variable (Y) for each ensemble member in each region. The following procedures were conducted:

i) We employed the variable clustering (VARCLUS) procedure to thoroughly assess collinearity among the variables. VARCLUS is a method that effectively segregates a set of numeric variables into disjoint or hierarchical clusters, each characterized by a linear combination of the variables within the cluster (Sarle, 1990). The criterion is that when the proportion of the variance explained by a cluster is larger than 0.8, it is advisable to select one variable from that cluster. Based on the results obtained from VARCLUS (Figs. S3 and S4), we made specific decisions to enhance the robustness of our analysis. For instance, we identified strong correlations exceeding 0.9 between potential ET and temperature (Tables S2-S13 in the Supplementary Information), as well as between soil moisture and TWS in all cases (except for the eastern NA (R5) in Tables S2-S13). Consequently, we chose to exclude potential ET and soil moisture from our analysis due to their high levels of correlation with temperature and TWS, respectively.

ii) We considered a linear regression model with potential independent variables (X): temperature, precipitation, real ET, and LAI. We conducted a temporal autocorrelation analysis on all the variables, including temperature, precipitation, real ET, and LAI data for each model. This analysis was carried out using the Autocorrelation function at a 95% confidence level. In all regions (except R4), the autocorrelation results indicated that the lags at the first and second months were statistically significant, while the third month lag was almost non-significant. Therefore, we modified the LMS model to include information from the two preceding months in these regions. However, in region R4, we observed different patterns. In this region, both real ET and temperature significantly depended on their respective conditions from the two previous months, while precipitation did not show this effect. Moreover, LAI in R4 exhibited dependencies on the first three and four preceding months under the SSP5-8.5 and SSP5-8.5-SAI scenarios, respectively. Consequently, we incorporated specific lagged months for each variable in R4.

iii) Identifying the outliers using the Bonferroni *p*-values (i.e., Bonferroni correlation) and then removing them. Bonferroni correlation is a modification for *p*-values when several dependent or independent statistical tests are being accomplished concurrently on a single data set. A Bonferroni correction divides the critical *p*-value by the number of comparisons being made (Bland and Altman, 1995). The number of outlier data points excluded varies from zero to 5 (over the 700 point) in the 36 models.

iv) Fitting the final model after removing the outliers. In all regions and scenarios, the MLR models are statistically significant at the 95% level. The variance explained (R^2) varies from around 0.3 in the dry southern MENA to 0.89 and 0.96 in the wetter lands around the Caspian and Mediterranean Seas.

v) Assessing the relative "importance" of the variables for TWS in the final model using the Lindeman, Merenda, and Gold (LMG) method (Lindeman et al., 1980), where the fractional variance accounted for is determined as the independent variable-order average over average contributions in models of different sizes. The LMG method considers the average contributions of each variable across different model sizes and then averages these averages to provide a more robust measure of variable importance. The LMG can be defined as (Grömping, 2007):

$$LMG(x_k) = \frac{1}{p!} \sum_{Permutation} seqR^2(\{x_k\} \mid r) \quad (4)$$

where $seqR^2(\{x_k\} \mid S_k(r)) = R^2(\{x_k\} \cup S_k(r)) - R^2(S_k(r))$ and

$$R^2(S) = \frac{Model\ SS(\mathrm{mod}\,el\ with\ regressors\ in\ set\ S)}{Total\ SS}$$

Orders have the same $S_k(r) = S$ summarize into a single summand, we therefore can re-write Eq. (4):

$$LMG(x_k) = \frac{1}{p!} \sum_{S \subseteq \{x_1,\ldots,x_p\} \setminus \{x_k\}} n(S)!(p - n(S) - 1)!\, seqR^2(\{x_k\} \mid S) \quad (5)$$

LMG has been recommended by Johnson and LeBreton (2004) and Grömping (2007) since it uses both direct effects and impacts adjusted for other regressors in the model. As the considered variables may be correlated with each other, when a new predictor is added to a model that already contains other predictors, its impact can be influenced by the presence of those other variables. The LMG method takes into account these interactions and adjusts the variable's contribution to reflect its unique impact while considering the effects of other regressors. Importance is a unitless variable and the sum of all independent variable importance's in each model equals the model's explained variance. Here we use all three ensemble members separately to estimate the robustness of the importance estimates.

3. Results:

3.1. Mean terrestrial water storage (TWS) changes due to GHG and SAI

In this section, we present the projected changes in TWS across MENA and the lands around the Caspian and Mediterranean Seas. We discuss trends in the TWS anomalies relative to TWS averaged over the historical period (1985-2014) in response to both GHG (SSP5-8.5) forcing and to GHG+SAI.

Figure 2 illustrates the original TWS anomalies, while Fig. S5 exclusively presents the long-term component, providing a clearer understanding of the changes under climate scenarios. The positive and negative anomalies in these figures refer to increasing and decreasing TWS, respectively. The trend decreases in the northern parts (R1 and R3) and eastern NA (R5) with a hyper-arid climate but rises in the Arabian Peninsula (R4) and western NA (R6) under both GHG and SAI scenarios, particularly over the latter part of the 21st century. In all regions, the SAI climate TWS is higher than SSP5-8.5 or at least lies in the across-range of SSP5-8.5 towards the end of the century, especially in R2 and R5 (Figs. 2 and S5). The TWS difference between SAI and global warming in the region R2, particularly over the latter part of the 21st century, is greater relative to the rest of the domain. The TWS change is smaller in the hyper-arid eastern NA (R5) than the other regions under both climate scenarios.

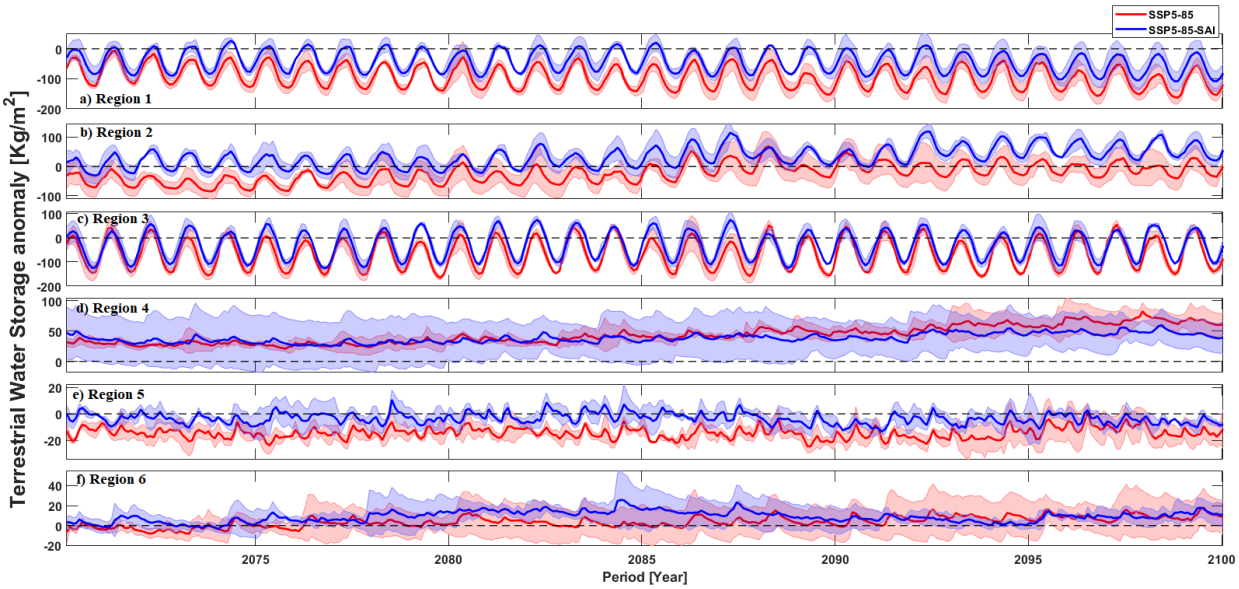

Figure 2. The TWS anomaly relative to the TWS averaged over the historical period across MENA and the lands around the Caspian and Mediterranean Seas under global warming without (SSP5-8.5) and with SAI (SSP5-8.5-SAI). Figures a-f respectively are for regions R1 to R6. Shading in each curve shows the across-ensemble range. The dashed line crossing the *y*-axis at zero in each subplot is the ensemble mean of TWS over the historical period (1985-2014).

Fig. 3 depicts the TWS differences between the historical (1985-2014) and the future climate scenarios over the 2071-2100 period. Consistent with the above findings, Figs. 3b and S6a-c show that the TWS response to GHG forcing in the wet regions around the Caspian (R1) and Mediterranean (R3) Seas is simulated as declining, while across the (semi)arid MENA region, particularly in central Iran (R2), the Arabian Peninsula (R4), and the southern portions of NA (R5 and R6), there is a positive trend. Under global warming, the largest decrease in TWS occurs around the Caspian (particularly in

the east) and the Mediterranean (except for its north) while its most robust increase happens in the southern margins of NA and the eastern parts of the Arabian Peninsula. SAI (Figs. 3c and S6d, e, and f) partially counteracts the changes imposed by the increased GHG emission, particularly in the wetter lands around the Caspian and Mediterranean Seas which are simulated as experiencing TWS decrease under global warming. Temporal-ensemble mean TWS due to GHG forcing (Fig. 3b) is only partially reversed by SAI (Fig. 3d), and the water storage shortfall is not fully canceled out by the intervention (Fig., 3c and d). However, simulated TWS in Iran and the southern half of MENA has greater water storage under SAI relative to the historical period (Fig. 3c).

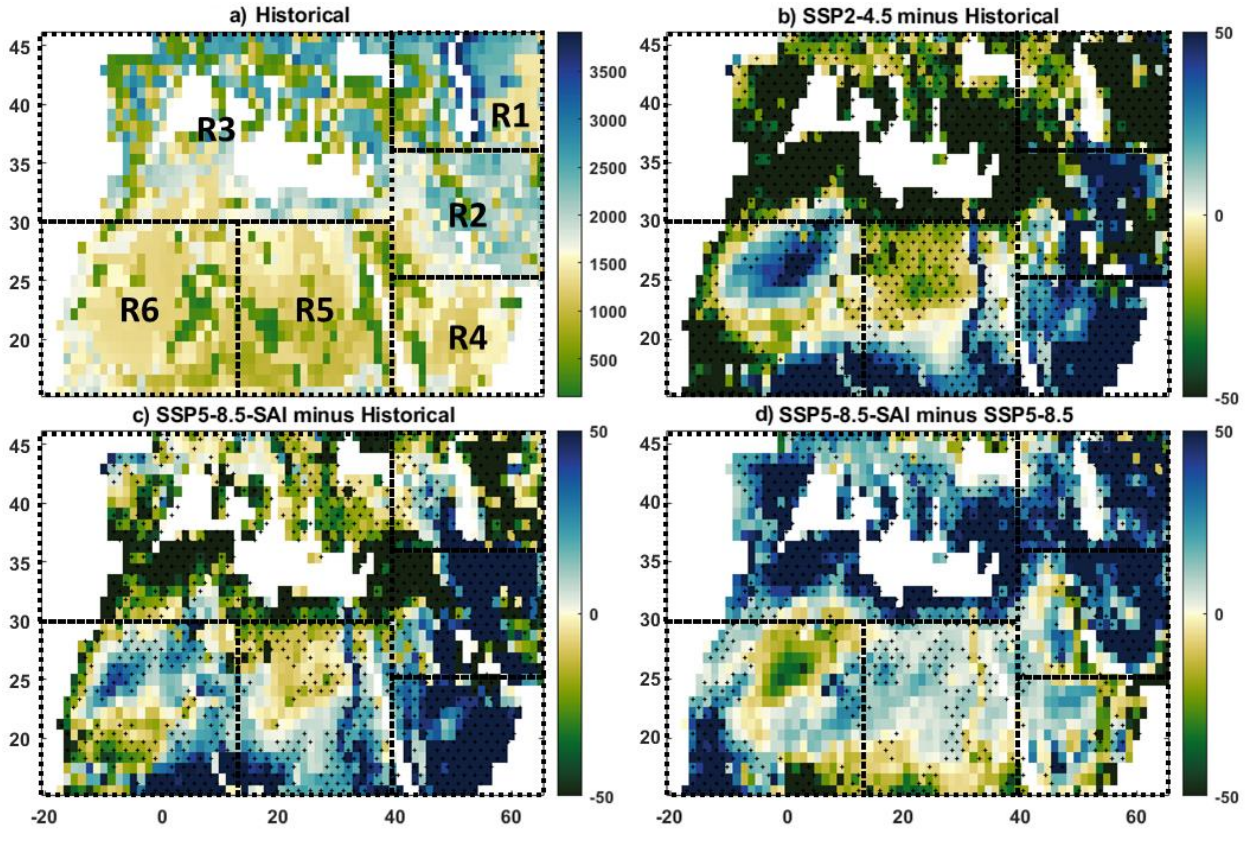

Figure 3. Ensemble mean maps of TWS across the studied domain in the historical climate (a) over 1985-2014 and their projected future changes in the 2071–2100 period under the SSP5-85 GHG scenario (SSP5-8.5 minus historical (b) and GHG+SAI minus historical (c)). The extent to which the SAI impacts the TWS changes imposed by global warming is further shown (SAI minus SSP5-8.5 (d)). Hatched areas show where all ensemble members agree on the sign of the changes.

In Fig. 4, we compare how simulated TWS statistical distributions vary between scenarios for each region. Mean TWS significantly ($p<0.05$) decreases in the wetter lands around the Caspian (R1) and Mediterranean (R3) Seas to the north (3.7-5.2% on area average) while it significantly increases in

the dry region of Arabian Peninsula (5.6%) in response to GHG warming. SAI, on the whole, partially reverses the projected changes in TWS from increasing GHG concentrations toward its historical values. Interestingly, SAI overcompensates the TWS changes imposed by the high GHG forcing in Iran and Iraq (R2) where this region shows no significant change under GHG emissions (Figs. 4b). SAI also has an amplifying effect in R5 and a slight overcompensation in R6, but its impact is statistically insignificant.

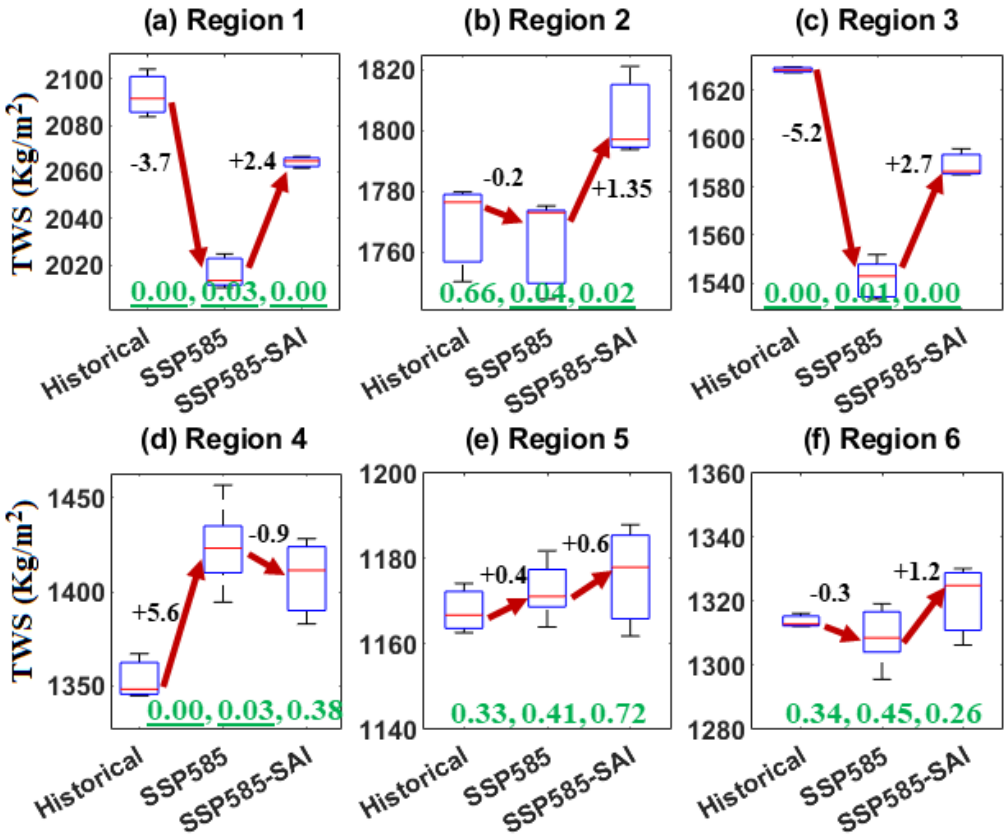

Figure 4. Box and whiskers plot of the changes in the Terrestrial Water Storage (TWS) in regions 1 to 6 over 2071-2100 under SSP5-8.5 and SSP5-8.5-SAI relative to historical conditions (1985-2014). The titles of each subplot refer to the regions. The median for each experiment is denoted by the red line, the upper (75th) and lower (25th) quartiles by the top and bottom of the box, and ensemble limits by the whisker extents. The positive/negative values in black are the change percent under SSP5-8.5 and SSP5-8.5-SAI relative to the median of the historical period data. The three values in green refer to *p*-values between historical and global warming, historical and SAI, and global warming and SAI, respectively, obtained from *t*-test analysis in which the underlined *p*-values are statistically significant.

We also compared the changes in TWS with changes in precipitation, temperature, real ET, soil moisture, and potential ET over each region under both global warming and SAI scenarios (Figs. S7

to S10 in the Supplementary Information). The TWS decreasing patterns under both SSP5-8.5 and SSP5-8.5-SAI scenarios across the entire study area are similar to soil moisture change patterns (Fig. S7 and S9 in Supplementary Information), but are more widespread than precipitation under global warming (Fig. S9). Notably, in the Mediterranean and the dry MENA region, the soil moisture variability accounts for the dominant component of TWS variability (Pokhrel et al., 2021). However, the decreased TWS is seen beyond the regions of reduced precipitation (Fig. S9), from beyond the Mediterranean and Atlantic coasts to include Syria, Iraq, and the lands around the Caspian Sea as well as to a wide portion of NA (Fig. 4). These include places where precipitation is either increasing or shows no significant change, consistent with results reported by Cook et al. (2020).

In Summary, our findings show that the SSP5-8.5-SAI scenario has a potential to partially offset the significant changes in mean TWS imposed by SSP5-8.5 over the entire MENA. While SAI (Fig. 3d) succeeded in reversing mean TWS deficits in the wetter lands around the Caspian and Mediterranean Seas driven by the GHG SSP5-8.5 scenario (Fig. 3b), it did not fully cancel out the TWS deficits (Figs. 3c, 4a, and 4c). However, in the dry MENA regions (Fig. 3d), particularly Iran (containing the Lut desert in the south-east region and the Kavir desert in the north-central), Iraq, and the Arabian Peninsula (housing the Arabian Desert), SAI resulted in higher mean water storage relative to the historical period (Figs. 3c and 4).

3.2 Changes in extreme TWS

We compared changes in the expected return frequency of comparatively rare events to those during the historical period. Changes in mean conditions discussed so far are clear, but the changes in extremes display even larger separations between those expected under pure GHG forcing and the GHG+SAI scenarios. An increase in the return level or decrease in the return period of TWS means that the rare levels of high water availability increase, while a decrease in return level for a given period means that rich water availability events become rarer. We applied a GEV distribution to the complete dataset of monthly TWS values without explicitly setting maximum values in Fig. 5. For comparison, we also extracted the annual maximum TWS values and provided the corresponding fitted GEV distribution. Overall, the probability densities for both datasets exhibit a high degree of similarity across various regions and scenarios (e.g., Figs. S11 and S12). Additionally, the graphs depicting return levels versus return periods based on annual maximums (Fig. S13) closely resemble the results obtained from the entire dataset (Fig. 5). In all cases, the trends are highly similar (compare Figs. 5 and S13), although it's worth noting that the annual maximums scenario exhibits

slightly wider upper and lower bounds compared to the entire dataset scenario. We therefore focus on the results obtained from the entire dataset. Fig. 5 shows the return levels versus return period curves with the 95% lower and upper bands. To determine which curves (including its upper and lower bounds) are significantly different from each other (*p*-values less than 0.05), we first conducted the repeated measures analysis of variance which compares means across one or more variables that are based on repeated observations, and then performed post hoc Tukey-Kramer comparisons. The expected return levels versus return period curves (Fig. 5) decrease in response to both GHG warming and GHG+SAI in the Caspian and Mediterranean Seas area (R1 and R3) as well as in the eastern NA (R5) as a more continental dry land but increase in the Arabian Peninsula (R4) and western NA (R6). In Iran and Iraq (R2), SAI leads to a significant increase in expected TWS return levels relative to both historical conditions and the high GHG emission scenarios (Fig. 5b) while SAI tends to partially counteract the GHG-driven TWS changes in R1, R3, R4, and R5. Larger TWS levels are expected for the entire MENA compared with the GHG climate alone, particularly in Iran, Iraq, and the western NA. Nonetheless, compared to the historical period, the Arabian Peninsula (Fig. 5d) is the region with the most robust increase in the extreme TWS under both the global warming and SAI scenarios. Extreme TWS in its neighbor dry land of eastern NA with a hyper-arid climate is still smaller than the historical conditions.

Table 2 quantitatively compares the differences between TWS (and its corresponding 95% lower and upper bounds in Fig. 5) changes at 30-, 50-, and 100-yr return periods under historical, global warming, and SAI scenarios. Global warming, on the whole, decreases the TWS extremes (i.e., fewer wetter conditions) at 30- to 100-year return periods over all the study areas except for the Arabian Peninsula (R4) and western NA (R6). The most robust decreases in the extreme TWS imposed by global warming relative to historical conditions occur in the lands around the Caspian R1 (-108% on average over return periods from 30- to 100-year) and Mediterranean R3 (-43% on average) and the eastern NA R5 (-89% on average) are partially suppressed by SAI. A small increase in the extreme TWS in Iran and Iraq (R2) simulated under GHG (+15%) is overcompensated by SAI (+57%). Although SAI decreases the TWS in the Arabian Peninsula (-11%) relative to global warming, it still tends to experience the most robust extreme water storage increases in the future (+153%) compared with historical conditions. In western NA, the SAI simulation slightly intensifies the increased extreme TWS imposed by high GHG emissions by +27%. Although SAI partially compensates for the changes over most of the study area (positive SSP5-8.5-SAI minus SSP5-8.5 values in Table 2), on the whole, extreme TWS tend to increase in the dry regions of Iran and Iraq,

the Arabian Peninsula, and western NA while substantially decreasing in the wetter lands around the Caspian and Mediterranean Seas, and to lower degrees, in the eastern NA as a more continental dry land compared with historical conditions.

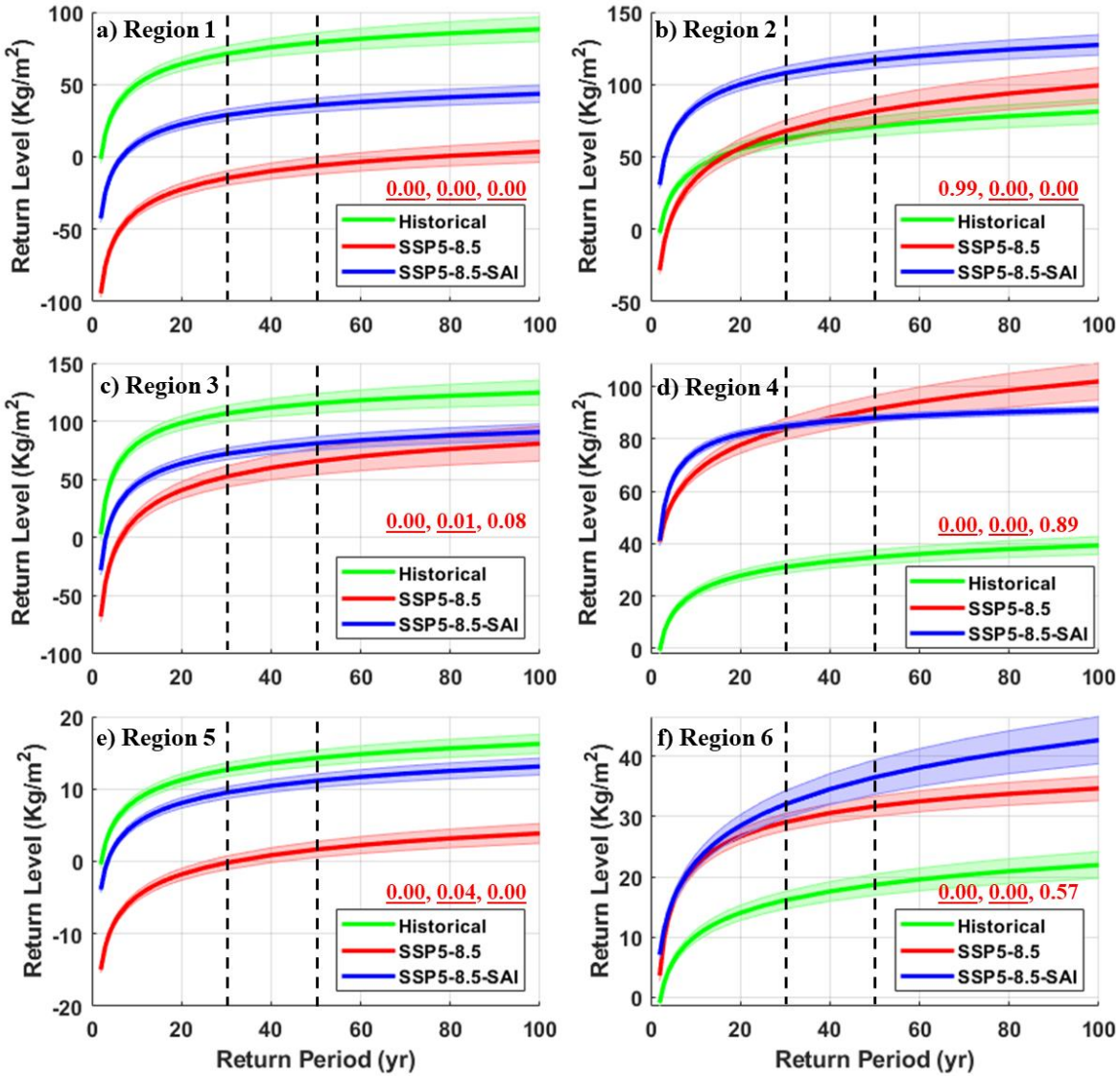

Figure 5. The TWS anomaly return level versus return period using the first three realizations for the historical, SSP5-8.5, and SSP5-8.5-SAI in regions 1 to 6 (a to f). The two parallel dashed black lines refer to 30- (left) and 50-year (right) return periods. Shading in each curve is the 95% upper and lower confidence bands. The three values in red refer to *p*-values between historical and global warming, historical and SAI, and global warming and SAI, respectively, obtained from the repeated measures analysis of variance and the post hoc Tukey-Kramer comparisons in which the underlined *p*-values are statistically significant.

Table 2. The percent differences (%) between the medians of the TWS return level at 30-, 50-, and 100-year return periods using the first three realizations for the historical, SSP5-8.5, and SSP5-8.5-SAI. Consistently, the value inside the parenthesis is the percent difference-range values between lowers and uppers 95% confidence intervals from different scenarios.

	(SSP5-8.5 − Historical)/Historical*100			(SSP5-8.5-SAI − Historical)/Historical*100			(SSP5-8.5-SAI − SSP5-8.5)/Historical*100		
Region	30-yr	50-yr	100-yr	30-yr	50-yr	100-yr	30-yr	50-yr	100-yr
R1	−121 (-130, -113)	-108 (-117, -100)	-96 (-105, -88)	−59 (-62, -57)	-55 (-57, -53)	-51 (-53, -49)	61 (56, 68)	53 (48, 60)	45 (40, 52)
R2	8 (6, 11)	15 (12, 17)	22 (20, 24)	73 (66, 81)	65 (58, 73)	57 (50, 65)	64 (55, 75)	50 (41, 60)	34 (25, 46)
R3	-51 (-56, -46)	-43 (-49, -38)	-35 (-42, -29)	-33 (-34, -32)	-30 (-31, -29)	-27 (-28, -26)	18 (14, 24)	13 (8, 20)	8 (2, 16)
R4	170 (163, 178)	163 (157, 169)	160 (155, 164)	173 (158, 191)	153 (138, 170)	132 (117, 150)	4 (-4, 13)	-10 (-19, 1)	-27 (-39, -14)
R5	-102 (-110, -95)	-89 (-96, -82)	-76 (-83, -70)	-25 (-26, -24)	-22 (-23, -21)	-19 (-20, -18)	77 (70, 84)	67 (61, 73)	57 (52, 63)
R6	80 (73, 89)	70 (63, 77)	58 (52, 65)	99 (95, 103)	95 (93, 99)	94 (93, 96)	18 (14, 22)	26 (21, 30)	36 (31, 41)

3.3 Drivers of TWS change

To assess which variables have the most impact on mean TWS under both global warming and SAI, we fitted an MLR model to each ensemble member separately in each of the six regions (Figs. 6 and 7). The most important variable for the mean TWS under both global warming and SAI scenarios is region-specific. In the wet lands surrounding the Caspian (R1) and Mediterranean (R3) Seas, temperature and precipitation are the primary drivers of TWS changes. In contrast, in the Middle East, characterized by predominantly dry climates (R2 and R4), vegetation coverage (i.e., LAI) plays a dominant role. This observation aligns with the fact that temperature limits ET in the wet regions, while in arid and hot regions, the availability of water for ET is the predominant limiting factor (Bao et al., 2021). In NA, where TWS changes are irregular, temperature holds the greatest significance in the eastern regions (R5), while real ET is the primary driver in the west (R6). Warmer climate enhances the atmospheric water content over regions and seasons (Cook et al., 2020) since 1°C warming is accompanied by ~7% enhancement in the air water storage capacity (Trenberth, 2011), and, in turn, increases the evaporative demand (Arnell, 1999), and vice versa for cooler conditions. Real ET itself is mostly controlled by temperature and available water for evaporation (i.e., precipitation, soil moisture, and vegetation coverage). With just temperature and precipitation as independent variables, we find that the temperature under both global warming and SAI is generally more important for TWS than precipitation over the wet lands around the Caspian and

Mediterranean Seas as well as the eastern NA. In contrast, precipitation plays a stronger role on TWS in Iran, Iraq, and the western NA with lower precipitation under both future climate scenarios.

The regression models indicate that TWS is mostly driven by the combined impacts of changes in vegetation coverage, real ET, temperature and precipitation, consistent with the fact that precipitation is not the only controlling factor for water resources (Cook et al., 2014; Wu et al., 2020). However, the temperature in the Mediterranean area with the highest precipitation over the entire domain studied plays a more important role than precipitation, vegetation coverage, and real ET under both warming and SAI scenarios.

Caution is required when interpreting the relative importance results for the arid regions of R4 to R6 as their variance explained (R^2=0.3 to 0.52) from the MLR models is smaller than those (up to 0.89 and 0.96) for the wetter lands around the Caspian and Mediterranean Seas. This, most probably, arises from the arid to hyper-arid climate of R4 to R6 with a small and irregular annual precipitation, and, in turn, irregular TWS anomaly time series (Figs. 2d, e, and f).

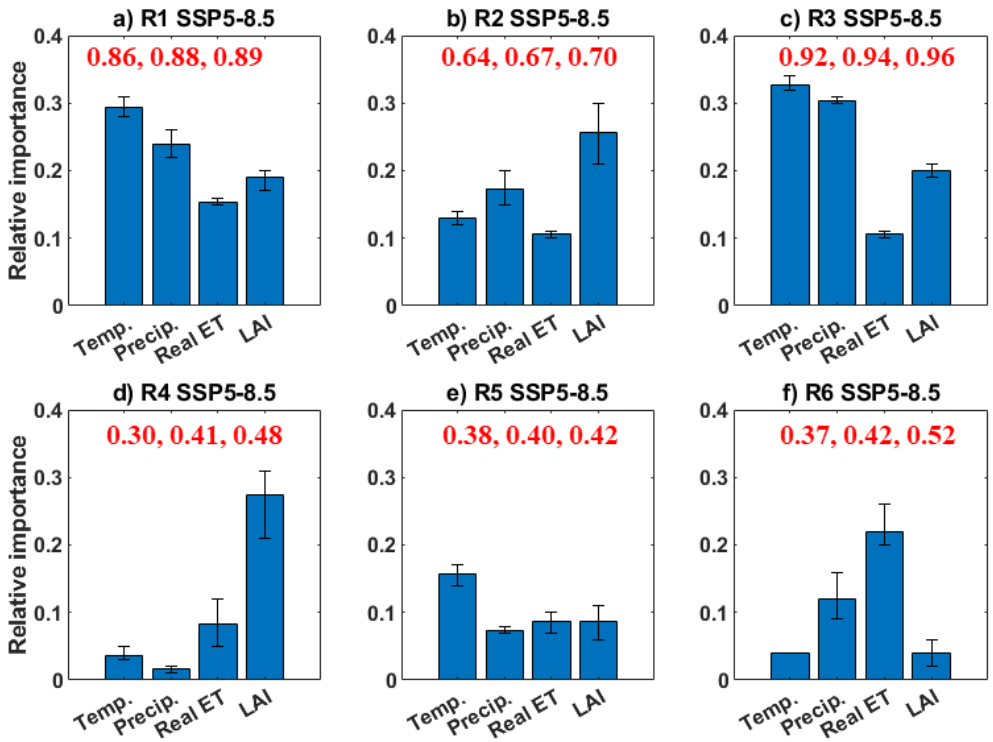

Figure 6. LMG importance plot (Lindeman et al., 1980) of the four independent variables in the regression for TWS for the global warming SSP5-8.5 scenario in each region. The bar and range-bar respectively show the ensemble mean importance and the range of importance from the three

ensemble members. The three values in red on each subplot shows the minimum, mean, and maximum variances explained by models.

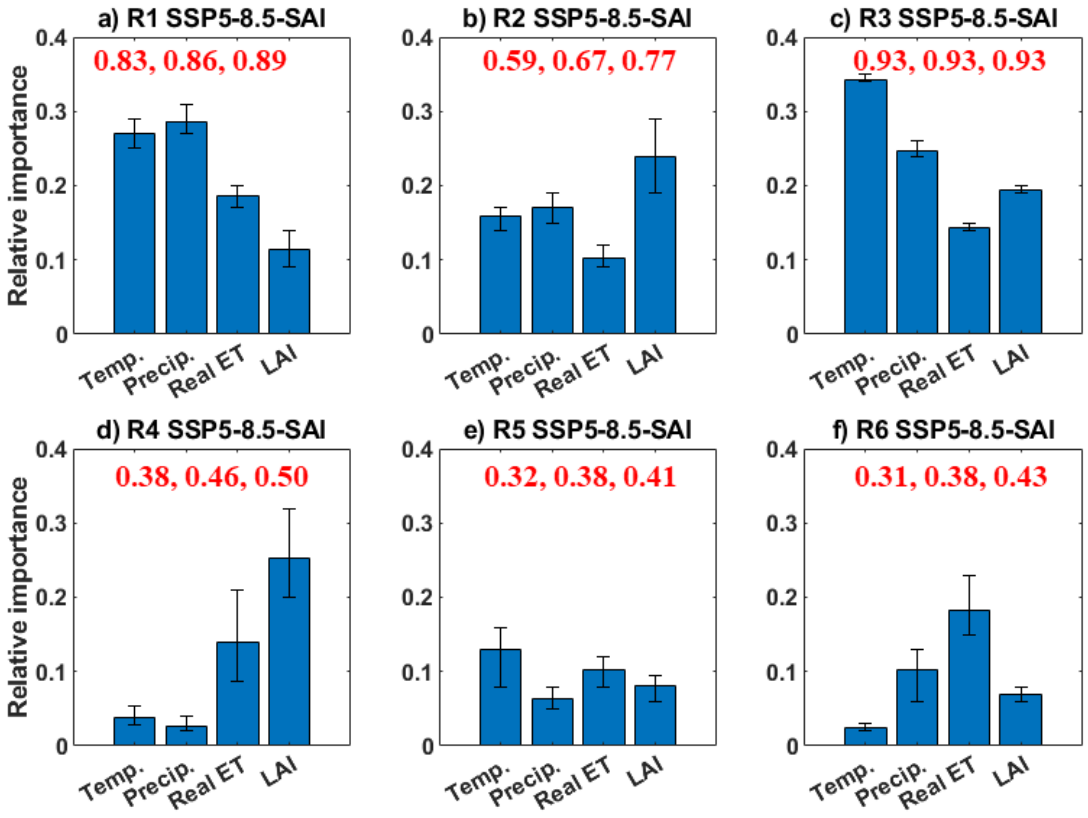

Figure 7. As in Fig. 6, but for the SSP5-8.5-SAI scenario.

4. Discussion

We have analyzed the potential impacts of the unmitigated global warming SSP5-8.5 scenario (GHG) and the same GHG emissions trajectory with the addition of SAI (GHG+SAI) on both the mean and extreme water storage across the lands around the Caspian and Mediterranean Seas, Middle East, and NA. We have used the CESM2(WACCM) climate model simulations with three realizations of each historic and SSP5-8.5-SAI scenario and five available realizations for SSP5-8.5. In response to high GHG emission over the 2071-2100 period, the mean TWS decreases in the wetter regions (i.e., around the Caspian and Mediterranean Seas with mild wet winters and warm to hot, dry summers), in agreement with the previous studies based on SSP5-8.5 (e.g., Cook et al., 2020; Scanlon et al., 2023), RCP2.6 and RCP4.5 (e.g., Döll et al., 2018) as well as with projections from 11 global hydrological models (Schewe et al., 2014) with globally forced 2°C warming (Schleussner et al., 2016). Similarly, a decrease in precipitation (Kim and Byun, 2009), surface runoff (Cook et al., 2020), and TWS

(Pokhrel et al., 2021) has been reported across Mediterranean coasts under GHG warming. In contrast, the mean TWS increases or shows no significant change in the MENA, housing several major deserts with minimal precipitation. The temporal-ensemble mean TWS increase in the southern MENA is consistent with other climate model simulations showing increased precipitation and soil moisture in CMIP6 simulations under SSP5-8.5 (Cook et al., 2020), and SSP2-4.5 (Ajjur et al., 2021; Scanlon et al., 2023). This further aligns with a projected northward shift of the inter-tropical convergence zone (ITCZ) in eastern Africa, mostly during a months of May to October (Mamalakis et al., 2021), leading to increased moisture transfer to the Southern Middle East and NA (Waha et al., 2017).

Given the prevailing water scarcity challenges in many regions of the Middle East where population growth is a continuing concern (Oroud, 2008), by mitigating the vulnerability to global warming, SAI may offer a potential strategy to augment the regional water resources across the area, particularly in the dry regions of Iran (containing the Lut desert in the south-east region and the Kavir desert in the north-central), Iraq, and the Arabian Peninsula (housing the Arabian Desert), as compared with the pure GHG forced scenario. Similarity, Jones et al. (2018) found that SAI could effectively counteract the changes in available water imposed by global warming on Earth's lands. Mousavi et al. (2023) also found increased soil moisture and enhanced vegetation coverage would lead to the reduction of dust concentration in the MEAN region under SAI.

The more robust and widespread deficit in mean TWS compared to precipitation in the area, which is in line with results reported by Cook et al. (2020), highlights the profound roles that other variables/processes have on the increased ET such as greater atmospheric moisture demand (Dai et al., 2013, 2018) and greater vegetation water use (Mankin et al., 2019) owing to warmer conditions under global warming, consistent with regression model results. According to MLR model results (Figs. 6 and 7), the projected changes in TWS were not solely attributable to precipitation; its interplay with other factors, such as vegetation coverage, temperature, and ET play a pivotal role. The vegetation coverage as the primary variable influencing changes in TWS in the MENA region substantially increases under global warming (Figs. S14 and S15). It has an important, but often complex and uncertain, role in surface water content (Lemordant et al., 2018; Trugman et al., 2018); the denser vegetation coverage, the higher evapotranspiration rates. Furthermore, although precipitation over a broad portion of MENA is lowered under SAI relative to global warming, the mean TWS, in general, increases across a broad portion of the MENA region in response to the

intervention. TWS significantly increases over Iran and Iraq under SAI compared to historical and global warming (Fig. 4b) as gains in available water from decreased temperature and, in turn, ET is largely sufficient to compensate for decreased precipitation (Figs. S8 and S10), signifying that in addition to precipitation, the water storage also strongly depends on local temperature (Ajjur et al., 2021). As an example, around the Caspian Sea (R1), although the changes in precipitation imposed by global warming are simulated to have been fully restored by SAI, the temperature has not; and in turn, the TWS is not fully restored by SAI. This is consistent with MLR model results (Fig. 7a) in which, beyond the precipitation, temperature also plays an important role in TWS across R1. Other studies also found that changes in precipitation does not necessarily correlate with changes in surface water, due to differences in precipitation and evaporation responses under SAI (Irvine et al., 2016).

Our findings, on the whole, suggest that the specific SAI scenario considered here could help water storage in the dry regions (R2, R4, R5, and R6), i.e., leads to higher soil moisture and TWS compared with both the historical conditions and pure GHG-induced global warming. Likewise, Dagon and Scharg (2017) documented a rise in mean water availability and soil moisture during a period of June to August in MENA using SolarGeo simulations, consistent with the significant reduction in daily maximum temperatures and ET across the Middle East. This works through the combined positive effects of (1) a substantial decrease in temperature and ET over the entire study area compared with SSP5-8.5 global warming, and (2) the increased precipitation in the southern MENA dry regions relative to historical conditions. The Middle East may therefore benefit from the water enrichment from climate change through the implementation of solar intervention (Burnell, 2021). However, the wet and colder regions, particularly around the Mediterranean coasts, may have less water storage compared with the historical period but more water relative to the GHG scenario due to a significant decrease in ET under SAI. Simpson et al. (2019) also reported a noteworthy decline of 18.5% in available water (precipitation minus evaporation) across the Mediterranean area under high GHG emissions while it has been partially reversed (only 5%) by a decrease in evaporation under SAI.

Although SAI partially compensates for the extreme TWS changes in most of the study area, aligning with findings by Jones et al. (2018), the overall extreme TWS trend indicates an increase in dry regions of Iran and Iraq, Arabian Peninsula, and western NA. Conversely, there is a substantial decrease in extreme TWS in the wetter lands around the Caspian and Mediterranean Seas, and to lower degrees, in the eastern NA compared to historical conditions. The implications of our findings under both future climate scenarios (SSP5-8.5 and SSP5-8.5-SAI) extend beyond hydrology and

water resources management. Changes in TWS have significant implications for climate adaptation, flood and drought risk management, and infrastructure planning. Some dry areas such as Iran, Iraq, and the Arabian Peninsula are projected to receive greater extreme TWS under both global warming and SAI or only SAI, and these regions have suffered historically from flooding (e.g., Abbaspour et al., 2009; Ghavidel and Jafari Hombari, 2020; Dezfuli et al., 2021). The significant increase in extreme TWS enhances their flood risks. Hence, governments in these regions should plan for adaptations to water megastructures such as the dams on the large rivers of Karkheh and Karun in western Iran and the Euphrates and Tigris in Iraq, since they have been mostly designed with historical hydrology in mind.

There are several caveats and caution needed for our results. First, our findings are based on a single model simulation (CESM2) and a single scenario climate scenario SSP5-8.5 with (three available realizations) and without (five available realizations) SAI. Future studies should consider alternative SAI scenarios to explore the sensitivity of our results to model and scenario choices. The SSP scenarios include some that clearly portray undesirable futures, especially the high emissions SSP5 scenarios or the regional rivalry SSP3 that illustrate the danger of unchecked climate change (MacMartin et al., 2022). There are more caveats for the SAI experiment used here (1) it deploys in 2020, therefore does not simulate any plausible future, and (2) takes into account solely the high-emissions scenario SSP5-8.5 that is suitable for capturing a high "signal" compared to internal variability. This is useful for understanding the science but inconsistent with present-day projections of mitigation attempts (Burgess et al., 2020). However, while the signal is stronger under high GHG emissions, it is plausible that the directions and patterns of response would be similar in a lower-emission experiment, with the magnitude of changes roughly depending on the degree of warming being suppressed by SAI (e.g., MacMartin et al., 2019).

5. Conclusions

The current study is the first attempt for understanding the influence of GHG emission and SAI scenarios on both mean and extreme water storage changes over the lands around the Caspian and Mediterranean Seas, Middle East, and northern Africa under global warming and SAI scenarios compared to the historical 1985-2014 conditions. The mean TWS is projected to decrease across the wetter lands around the Caspian and Mediterranean Seas to the north (3.7-5.2% on average) but increase over the most MENA region (up to 5.6% over the Arabian Peninsula) that has a drier climate under the high GHG forcing compared to the present-day conditions.

Although the SAI tends to reverse, to a degree, the significant changes in TWS revealed by SSP5-8.5 over the entire area, it significantly overcompensates for the slightly reduced TWS under the high GHG scenario in Iran and Iraq. MLR model analysis of driving factors suggests that the impacts of temperature on water storage changes, like precipitation, are also important under both high GHG forcing and SAI scenarios. Although SAI mostly decreases precipitation over most of the domain, it is accompanied by higher mean TWS across the entire study area due to the cooler climate.

Although significant changes in the extreme TWS under high GHG emissions are reduced by SAI, the changes due to both future climate changes are still large relative to the historical period across a broad portion of the domain. With SAI, TWS significantly decreases in the eastern lands around the Caspian Sea while substantially increasing across the Middle East regions of Iran, Iraq, and the Arabian Peninsula. This may increase flood risks since water megastructures have been mostly designed with historical hydrology in mind. Finally, the SAI scenario appears to increase accessible water storage in the dry regions of the Middle East and northern Africa. The wetter and colder lands around the Caspian and Mediterranean Seas may have less available water compared with the historical conditions, although SAI partially ameliorates the changes imposed by global warming.

Data availability:

The data for CESM2 simulations are publicly available via its website: https://esgf-node.llnl.gov/search/cmip6/. To access these specific data via ESGF website use the Source ID = CESM2-WACCM, Experiment ID=ssp585, and Frequency = mon. The SSP5-8.5-SAI data are freely available at https://www.earthsystemgrid.org/dataset/ucar.cgd.ccsm4.geomip.ssp5.html (https://doi.org/10.26024/t49k-1016).

Acknowledgments:

We appreciate the financial support from the DEGREES Initiative in collaboration with the World Academy of Sciences (TWAS) under grant no. 4500443035.

Author contributions:

AR: coordinated the analysis, graphics of various figures, and manuscript preparation; KK and ST: conceptualized and prepared the data; and JCM: conceptualized and coordinated the interpretation and discussion for various sections. All authors contributed to the discussion and writing.

Competing the Interest:

The contact author has declared that none of the authors has any competing interests.

Financial support:

This research has been supported by the DEGREES Initiative in collaboration with the World Academy of Sciences (grant no. 4500443035).

References:

Abbaspour, K. C., Faramarzi, M., Ghasemi, S. S., & Yang, H. (2009). Assessing the impact of climate change on water resources in Iran. Water resources research, 45(10).

Abdelmoaty, H. M., Papalexiou, S. M., Rajulapati, C. R., & AghaKouchak, A. (2021). Biases beyond the mean in CMIP6 extreme precipitation: A global investigation, Earths Future, 9, e2021EF002196.

Abiodun, B. J., Odoulami, R. C., Sawadogo, W., Oloniyo, O. A., Abatan, A. A., New, M., ... & MacMartin, D. G. (2021). Potential impacts of stratospheric aerosol injection on drought risk managements over major river basins in Africa. Climatic Change, 169(3), 1-19.

Ajjur, S. B., & Al-Ghamdi, S. G. (2021). Evapotranspiration and water availability response to climate change in the Middle East and North Africa. Climatic Change, 166(3-4), 28.

Arjdal, K., Driouech, F., Vignon, E., Chéruy, F., Manzanas, R., Drobinski, P., ... & Idelkadi, A. (2023). Future of land surface water availability over the Mediterranean basin and North Africa: Analysis and synthesis from the CMIP6 exercise. Atmospheric Science Letters, e1180.

Arnell, N. W. (1999). Climate change and global water resources. Global environmental change, 9, S31-S49.

Azzopardi, B., Balzan, M. V., Cherif, S., Doblas-Miranda, E., dos Santos, M., Dobrinski, P., ... & Xoplaki, E. (2020). Climate and environmental change in the Mediterranean basin–current situation and risks for the future. First Mediterranean assessment report.

735 Babaousmail, H., Hou, R., Ayugi, B., Ojara, M., Ngoma, H., Karim, R., ... & Ongoma, V. (2021). Evaluation
736 of the performance of CMIP6 models in reproducing rainfall patterns over North
737 Africa. Atmosphere, 12(4), 475.
738 Bağçaci, S. Ç., Yucel, I., Duzenli, E., & Yilmaz, M. T. (2021). Intercomparison of the expected change in
739 the temperature and the precipitation retrieved from CMIP6 and CMIP5 climate projections:
740 A Mediterranean hot spot case, Turkey. Atmospheric Research, 256, 105576.
741 Bala, G., Duffy, P. B., & Taylor, K. E. (2008). Impact of geoengineering schemes on the global
742 hydrological cycle. Proceedings of the National Academy of Sciences, 105(22), 7664-7669.
743 Bao, Y., Duan, L., Liu, T., Tong, X., Wang, G., Lei, H., ... & Singh, V. P. (2021). Simulation of
744 evapotranspiration and its components for the mobile dune using an improved dual-source
745 model in semi-arid regions. Journal of Hydrology, 592, 125796.
746 Barlow, M., Zaitchik, B., Paz, S., Black, E., Evans, J., & Hoell, A. (2016). A review of drought in the Middle
747 East and southwest Asia. Journal of climate, 29(23), 8547-8574.
748 Bland, J. M., & Altman, D. G. (1995). Multiple significance tests: the Bonferroni
749 method. Bmj, 310(6973), 170.
750 Bucchignani, E., Mercogliano, P., Panitz, H.-J., & Montesarchio, M. (2018). Climate change projections
751 for the Middle East–North Africa domain with COSMO-CLM at different spatial resolutions.
752 Advances in Climate Change Research, 9(1), 66–80. https://doi.org/10.1016/j.
753 Accre.2018.01.004
754 Burgess, M. G., Ritchie, J., Shapland, J., & Pielke, R. (2020). IPCC baseline scenarios have over-projected
755 CO2 emissions and economic growth. Environmental Research Letters, 16(1), 014016.
756 Burnell, L. (2021). Risks to global water resources from geoengineering the climate with solar
757 radiation management (Doctoral dissertation, University of Nottingham).
758 Byun, H. R., & Wilhite, D. A. (1999). Objective quantification of drought severity and duration. Journal
759 of climate, 12(9), 2747-2756.
760 Cook, B. I., Mankin, J. S., Marvel, K., Williams, A. P., Smerdon, J. E., & Anchukaitis, K. J. (2020). Twenty-
761 first century drought projections in the CMIP6 forcing scenarios. Earth's Future. 8,
762 e2019EF001461.
763 Cook, B. I., Anchukaitis, K. J., Touchan, R., Meko, D. M., & Cook, E. R. (2016). Spatiotemporal drought
764 variability in the Mediterranean over the last 900 years. Journal of Geophysical Research:
765 Atmospheres, 121(5), 2060-2074.
766 Cook, B. I., Smerdon, J. E., Seager, R., & Coats, S. (2014). Global warming and 21 st century
767 drying. Climate dynamics, 43, 2607-2627.

768 Crook, J. A., Jackson, L. S., Osprey, S. M., & Forster, P. M. (2015). A comparison of temperature and
769 precipitation responses to different Earth radiation management geoengineering
770 schemes. Journal of Geophysical Research: Atmospheres, 120(18), 9352-9373.
771 Cheng, W., MacMartin, D. G., Dagon, K., Kravitz, B., Tilmes, S., Richter, J. H., ... & Simpson, I. R. (2019).
772 Soil moisture and other hydrological changes in a stratospheric aerosol geoengineering large
773 ensemble. Journal of Geophysical Research: Atmospheres, 124(23), 12773-12793.
774 Dai, A. (2013). Increasing drought under global warming in observations and models. Nature climate
775 change, 3(1), 52-58.
776 Dagon, K., & Schrag, D. P. (2017). Regional climate variability under model simulations of solar
777 geoengineering. Journal of Geophysical Research: Atmospheres, 122(22), 12-106.
778 Danabasoglu, G., Lamarque, J. F., Bacmeister, J., Bailey, D. A., DuVivier, A. K., Edwards, J., ... & Strand,
779 W. G. (2020). The community earth system model version 2 (CESM2). Journal of Advances in
780 Modeling Earth Systems, 12(2), e2019MS001916.
781 Dezfuli, A., Bosilovich, M. G., & Barahona, D. (2021). A dusty atmospheric river brings floods to the
782 Middle East. Geophysical Research Letters, 48(23), e2021GL095441.
783 Dagon, K., & Schrag, D. P. (2016). Exploring the effects of solar radiation management on water
784 cycling in a coupled land–atmosphere model. Journal of Climate, 29(7), 2635-2650.
785 Doksum, K. A., & Sievers, G. L. (1976). Plotting with confidence: Graphical comparisons of two
786 populations. Biometrika, 63(3), 421-434.
787 Döll, P., Trautmann, T., Gerten, D., Schmied, H. M., Ostberg, S., Saaed, F., & Schleussner, C. F. (2018).
788 Risks for the global freshwater system at 1.5 C and 2 C global warming. Environmental
789 Research Letters, 13(4), 044038.
790 Döll, P.; Flörke, M. Global-Scale Estimation of Diffuse Groundwater Recharge; Institute of Physical
791 Geography, Frankfurt University: Frankfurt am Main, Germany, 2005; Available online:
792 https://www.uni-frankfurt.de/45217767/FHP_03_Doell_Floerke_2005.pdf.
793 Droogers, P., Immerzeel, W. W., Terink, W., Hoogeveen, J., Bierkens, M. F. P., Van Beek, L. P. H., &
794 Debele, B. (2012). Water resources trends in Middle East and North Africa towards
795 2050. Hydrology and Earth System Sciences, 16(9), 3101-3114.
796 Evans, J. P., & Smith, R. B. (2006). Water vapor transport and the production of precipitation in the
797 eastern Fertile Crescent. Journal of Hydrometeorology, 7(6), 1295-1307.
798 Eyring, V., Bony, S., Meehl, G. A., Senior, C. A., Stevens, B., Stouffer, R. J., & Taylor, K. E. (2016). Overview
799 of the Coupled Model Intercomparison Project Phase 6 (CMIP6) experimental design and
800 organization. Geoscientific Model Development, 9(5), 1937-1958.

Fader M., Shi S., Von Bloh W., Bondeau A., Cramer W. (2016). Mediterranean irrigation under climate change: More efficient irrigation needed to compensate for increases in irrigation water requirements. Hydrol. Earth Syst. Sci. 20, 953–973. doi: 10.5194/hess-20-953-2016

Famiglietti, J. S. (2014). The global groundwater crisis. Nature Climate Change, 4(11), 945-948.

Faour, G., Mhawej, M., & Fayad, A. (2016). Detecting changes in vegetation trends in the Middle East and North Africa (MENA) region using SPOT vegetation. Cybergeo: European Journal of Geography.

Fragaszy, S. R., Jedd, T., Wall, N., Knutson, C., Fraj, M. B., Bergaoui, K., ... & McDonnell, R. (2020). Drought Monitoring and Warning System for the Middle East and North Africa. Bulletin of the American Meteorological Society, 101(10), 904-910.

Ghavidel, Y., & Jafari Hombari, F. (2020). Synoptic analysis of unexampled super-heavy rainfall on April 1, 2019, in west of Iran. Natural hazards, 104(2), 1567-1580.

Gilleland, E. (2020). Bootstrap methods for statistical inference. Part II: Extreme-value analysis. Journal of Atmospheric and Oceanic Technology, 37(11), 2135-2144.

Giorgi, F., & Lionello, P. (2008). Climate change projections for the Mediterranean region. Global and Planetary Change, 63(2-3), 90–104. https://doi.org/10.1016/j.gloplacha.2007.09.005

Giorgi F. (2006) Climate change hot-spots. Geophys Res Lett 33: L08707. doi:10.1029/2006GL025734.

Govindasamy B., Caldeira K. (2000) Geoengineering Earth's radiation balance to mitigate CO2-induced climate change. Geophys Res Lett 27:2141–2144.

Grömping, U. (2007). Relative importance for linear regression in R: the package relaimpo. Journal of statistical software, 17, 1-27.

Hobeichi, S., Abramowitz, G., Ukkola, A. M., De Kauwe, M., Pitman, A., Evans, J. P., & Beck, H. (2022). Reconciling historical changes in the hydrological cycle over land. npj Climate and Atmospheric Science, 5(1), 17.

Hofste, R. W., Reig, P., & Schleifer, L. (2019). 17 countries, home to one-quarter of the world's population, face extremely high water stress.

Intergovernmental Panel on Climate Change (IPCC): Working Group I Contribution to the Sixth Assessment Report (AR6), Climate Change 2021: The Physical Science Basis, 2021, https://www.ipcc.ch/assessment-report/ar6/ (last access: 5 December 2022), 2021.

Irvine, P. J., Kravitz, B., Lawrence, M. G., & Muri, H. (2016). An overview of the Earth system science of solar geoengineering. Wiley Interdisciplinary Reviews: Climate Change, 7(6), 815-833.

833 Johnson, J. W., & LeBreton, J. M. (2004). History and use of relative importance indices in
834 organizational research. Organizational research methods, 7(3), 238-257.
835 Jones, A. C., Hawcroft, M. K., Haywood, J. M., Jones, A., Guo, X., & Moore, J. C. (2018). Regional climate
836 impacts of stabilizing global warming at 1.5 K using solar geoengineering. Earth's
837 Future, 6(2), 230-251.
838 Karami, K., Tilmes, S., Muri, H., & Mousavi, S. V. (2020). Storm track changes in the Middle East and
839 North Africa under stratospheric aerosol geoengineering. Geophysical Research
840 Letters, 47(14), e2020GL086954.
841 Kim, D. W., & Byun, H. R. (2009). Future pattern of Asian drought under global warming
842 scenario. Theoretical and Applied Climatology, 98(1), 137-150.
843 Konapala, G., Mishra, A. K., Wada, Y., & Mann, M. E. (2020). Climate change will affect global water
844 availability through compounding changes in seasonal precipitation and evaporation. Nature
845 communications, 11(1), 3044.
846 Kravitz, B., et al. (2013), An energetic perspective on hydrological cycle changes in the
847 Geoengineering Model Intercomparison Project (GeoMIP), J. Geophys. Res. Atmos., 118,
848 13,087–13,102, doi:10.1002/2013JD020502
849 Lelieveld, J., Hadjinicolaou, P., Kostopoulou, E., Chenoweth, J., El Maayar, M., Giannakopoulos, C., ... &
850 Xoplaki, E. (2012). Climate change and impacts in the Eastern Mediterranean and the Middle
851 East. Climatic change, 114, 667-687.
852 Lemordant, L., Gentine, P., Swann, A. S., Cook, B. I., & Scheff, J. (2018). Critical impact of vegetation
853 physiology on the continental hydrologic cycle in response to increasing CO2. Proceedings of
854 the National Academy of Sciences, 115(16), 4093. https://doi.org/10.1073/
855 pnas.1720712115.
856 Lian, X., Piao, S., Chen, A., Huntingford, C., Fu, B., Li, L. Z., ... & Roderick, M. L. (2021). Multifaceted
857 characteristics of dryland aridity changes in a warming world. Nature Reviews Earth &
858 Environment, 2(4), 232-250.
859 Lindeman, R. H., Merenda, P. F., Gold, R. Z., (1980). Introduction to bivariate and multivariate
860 analysis (No. 04; QA278, L553.). Uniq ID: 5310754 Scott, Foresman, Glenview, IL.
861 Lionello, P., Malanotte-Rizzoli, P., Boscolo, R., Alpert, P., Artale, V., Li, L., ... & Xoplaki, E. (2006). The
862 Mediterranean climate: an overview of the main characteristics and issues. Developments in
863 earth and environmental sciences, 4, 1-26.

MacMartin, D. G., Visioni, D., Kravitz, B., Richter, J. H., Felgenhauer, T., Lee, W. R., ... & Sugiyama, M. (2022). Scenarios for modeling solar radiation modification. Proceedings of the National Academy of Sciences, 119(33), e2202230119.

Mamalakis, A., Randerson, J.T., Yu, J.-Y., Pritchard, M.S., Magnusdottir, G., Smyth, P. et al. (2021) Zonally opposing shifts of the intertropical convergence zone in response to climate change, 45.

Masson-Delmotte, V., Zhai, P., Pörtner, H. O., Roberts, D., Skea, J., & Shukla, P. R. (2022). Global Warming of 1.5° C: IPCC Special Report on Impacts of Global Warming of 1.5° C above Pre-industrial Levels in Context of Strengthening Response to Climate Change, Sustainable Development, and Efforts to Eradicate Poverty. Cambridge University Press.

Milly, P. C., Dunne, K. A., & Vecchia, A. V. (2005). Global pattern of trends in streamflow and water availability in a changing climate. Nature, 438(7066), 347-350.

Mooney, H., Cropper, A. & Reid, W. Confronting the human dilemma. Nature 434, 561–-562 (2005).

Mousavi, S. V., Karami, K., Tilmes, S., Muri, H., Xia, L., and Rezaei, A. (2023). Future dust concentration over the Middle East and North Africa region under global warming and stratospheric aerosol intervention scenarios, Atmos. Chem. Phys., 23, 10677–10695, https://doi.org/10.5194/acp-23-10677-2023

Muthyala, R., Bala, G., & Nalam, A. (2018). Regional scale analysis of climate extremes in an SRM geoengineering simulation, Part 1: precipitation extremes. Current Science, 1024-1035.

Nooni, I.K.; Ogou, F.K.; Chaibou, A.A.S.; Nakoty, F.M.; Gnitou, G.T.; Lu, J. (2023). Evaluating CMIP6 Historical Mean Precipitation over Africa and the Arabian Peninsula against Satellite-Based Observation. Atmosphere, 14, 607. https://doi.org/10.3390/atmos14030607Oroud, I. M. (2008). The impacts of climate change on water resources in Jordan. Climatic changes and water resources in the Middle East and North Africa, 109-123.

Peel, M. C., Finlayson, B. L., & McMahon, T. A. (2007). Updated world map of the Köppen-Geiger climate classification. Hydrology and earth system sciences, 11(5), 1633-1644.

Pokhrel, Y., Felfelani, F., Satoh, Y., Boulange, J., Burek, P., Gädeke, A., ... & Wada, Y. (2021). Global terrestrial water storage and drought severity under climate change. Nature Climate Change, 11(3), 226-233.

Ricke, K., Wan, J. S., Saenger, M., & Lutsko, N. J. (2023). Hydrological Consequences of Solar Geoengineering. Annual Review of Earth and Planetary Sciences, 51, 447-470.

Ricke, K. L., Morgan, M. G., & Allen, M. R. (2010). Regional climate response to solar-radiation management. Nature Geoscience, 3(8), 537-541.

Reiter, L., Falk, H., Groat, C. & Coussens, C. M. (eds) From Source Water to Drinking Water: Workshop Summary (National Academies Press, Washington DC, 2004).

Robock, A., Oman, L., & Stenchikov, G. L. (2008). Regional climate responses to geoengineering with tropical and Arctic SO2 injections. Journal of Geophysical Research: Atmospheres, 113(D16).

Sarle, W. (1990). The VARCLUS Procedure. In *SAS/STAT User's Guide* (fourth, Vol. 2, pp. 1641–1659). SAS Institute, Inc. http://support.sas.com/documentation/onlinedoc/stathttp://support.sas.com/documentation/onlinedoc/stat

Schewe, J., Heinke, J., Gerten, D., Haddeland, I., Arnell, N. W., Clark, D. B., Dankers, R., Eisner, S., Fekete, B. M., ColonGonzalez, F. J., Gosling, S. N., Kim, H., Liu, X., Masaki, Y., Portmann, F. T., Satoh, Y., Stacke, T., Tang, Q., Wada, Y., Wisser, D., Albrecht, T., Frieler, K., Piontek, F., Warszawski, L., and Kabat, P.: Multimodel assessment of water scarcity under climate change, P. Natl. Acad. Sci., 111, 3245–3250, doi:10.1073/pnas.1222460110, 2014

Shaban, A. (2008). Impact of climate change on water resources of Lebanon: Indications of hydrological droughts. Climatic changes and water resources in the Middle East and North Africa, 125-143.

Shiklomanov, I. A. & Rodda, J. C. (2003). (eds) World Water Resources at the Beginning of the 21st Century (Cambridge Univ. Press, Cambridge, 2003).

Simpson, I. R., Tilmes, S., Richter, J. H., Kravitz, B., MacMartin, D. G., Mills, M. J., ... & Pendergrass, A. G. (2019). The regional hydroclimate response to stratospheric sulfate geoengineering and the role of stratospheric heating. Journal of Geophysical Research: Atmospheres, 124(23), 12587-12616.

Scanlon, B. R., Fakhreddine, S., Rateb, A., de Graaf, I., Famiglietti, J., Gleeson, T., ... & Zheng, C. (2023). Global water resources and the role of groundwater in a resilient water future. Nature Reviews Earth & Environment, 1-15.

Schleussner, C. F., Lissner, T. K., Fischer, E. M., Wohland, J., Perrette, M., Golly, A., ... & Schaeffer, M. (2016). Differential climate impacts for policy-relevant limits to global warming: the case of 1.5 C and 2 C. Earth system dynamics, 7(2), 327-351.

Suppan, P., Kunstmann, H., Heckel, A., & Rimmer, A. (2008). Impact of climate change on water availability in the Near East. Climate changes and water resources in the Middle East and North Africa. Springer, Environmental Science and Engineering, Berlin.

Tabari, H., & Willems, P. (2018). Seasonally varying footprint of climate change on precipitation in the Middle East. Scientific reports, 8(1), 4435.

Tilmes, S., MacMartin, D. G., Lenaerts, J., Van Kampenhout, L., Muntjewerf, L., Xia, L., ... & Robock, A. (2020). Reaching 1.5 and 2.0 C global surface temperature targets using stratospheric aerosol geoengineering. Earth System Dynamics, 11(3), 579-601.

Tilmes, S., Richter, J.H., Mills, M.J., Kravitz, B., MacMartin, D.G., Garcia, R.R., Kinnison, D.E., Lamarque, J.F., Tribbia, J. and Vitt, F. (2018). Effects of different stratospheric SO2 injection altitudes on stratospheric chemistry and dynamics. Journal of Geophysical Research: Atmospheres, 123(9), pp.4654-4673.

Tilmes, S., Fasullo, J., Lamarque, J. F., Marsh, D. R., Mills, M., Alterskjær, K., ... & Watanabe, S. (2013). The hydrological impact of geoengineering in the Geoengineering Model Intercomparison Project (GeoMIP). Journal of Geophysical Research: Atmospheres, 118(19), 11-036.

Trenberth, K. E. (2011). Changes in precipitation with climate change. Climate research, 47(1-2), 123-138.

Trugman, A. T., Medvigy, D., Mankin, J. S., & Anderegg, W. R. L. (2018). Soil moisture stress as a major driver of carbon cycle uncertainty. Geophysical Research Letters, 45, 6495–6503. https://doi.org/10.1029/2018GL078131

Trautmann, T., Koirala, S., Carvalhais, N., Güntner, A., & Jung, M. (2022). The importance of vegetation in understanding terrestrial water storage variations. Hydrology and Earth System Sciences, 26(4), 1089-1109.

Visioni, D., MacMartin, D. G., Kravitz, B., Boucher, O., Jones, A., Lurton, T., Martine, M., Mills, M. J., Nabat, P., Niemeier, U., Séférian, R., and Tilmes, S.: Identifying the sources of uncertainty in climate model simulations of solar radiation modification with the G6sulfur and G6solar Geoengineering Model Intercomparison Project (GeoMIP) simulations, Atmos. Chem. Phys., 21, 10039–10063, https://doi.org/10.5194/acp-21-10039-2021, 2021.

Waha, K., Krummenauer, L., Adams, S., Aich, V., Baarsch, F., Coumou, D. et al. (2017) Climate change impacts in the Middle East and northern Africa (MENA) region and their implications for vulnerable population groups. Regional Environmental Change, 17(6), 1623–1638. Available from: https://doi.org/10.1007/s10113-017-1144-2

Wang, J., Song, C., Reager, J. T., Yao, F., Famiglietti, J. S., Sheng, Y., ... & Wada, Y. (2018). Recent global decline in endorheic basin water storages. Nature geoscience, 11(12), 926-932.

Wang, Z., Zhan, C., Ning, L., & Guo, H. (2021). Evaluation of global terrestrial evapotranspiration in CMIP6 models. Theoretical and Applied Climatology, 143, 521-531.

World Bank (2017). Beyond Scarcity: Water Security in the Middle East and North Africa. The World Bank.

963 Wu, W. Y., Lo, M. H., Wada, Y., Famiglietti, J. S., Reager, J. T., Yeh, P. J. F., ... & Yang, Z. L. (2020). Divergent
964 effects of climate change on future groundwater availability in key mid-latitude
965 aquifers. Nature communications, 11(1), 3710.
966 Wu, R. J., Lo, M. H., & Scanlon, B. R. (2021). The annual cycle of terrestrial water storage anomalies in
967 CMIP6 models evaluated against GRACE data. Journal of Climate, 34(20), 8205-8217.
968 United Nations Educational Scientific and Cultural Organization, UNESCO (2003). Water for People—
969 Water for Life, The United Nations World Water Development Report (Berghahn Books,
970 Oxford, 2003).
971 Xiong, J., Guo, S., Chen, J., & Yin, J. (2022). Global evaluation of the "dry gets drier, and wet gets wetter"
972 paradigm from a terrestrial water storage change perspective. Hydrology and Earth System
973 Sciences, 26(24), 6457-6476.
974 Zamani, Y., Hashemi Monfared, S. A., Azhdari Moghaddam, M., & Hamidianpour, M. (2020). A
975 comparison of CMIP6 and CMIP5 projections for precipitation to observational data: the case
976 of Northeastern Iran. Theoretical and Applied Climatology, 142, 1613-1623.
977 Zittis, G., Hadjinicolaou, P., Klangidou, M., Proestos, Y., & Lelieveld, J. (2019). A multi-model, multi-
978 scenario, and multi-domain analysis of regional climate projections for the
979 Mediterranean. Regional Environmental Change, 19(8), 2621-2635.
980 Zhang, X., Li, J., Wang, Z., & Dong, Q. (2022). Global hydroclimatic drivers of terrestrial water storage
981 changes in different climates. CATENA, 219, 106598.
982 Zhang, B., Xia, Y., Long, B., Hobbins, M., Zhao, X., Hain, C., ... & Anderson, M. C. (2020). Evaluation and
983 comparison of multiple evapotranspiration data models over the contiguous United States:
984 Implications for the next phase of NLDAS (NLDAS-Testbed) development. Agricultural and
985 Forest Meteorology, 280, 107810.
986